

# Neutrino mass parameters from Kamland, SNO and other solar evidence

P. Aliani<sup>ab\*</sup>, V. Antonelli<sup>a\*</sup>, M. Picariello<sup>a\*</sup>, E. Torrente-Lujan<sup>c\*</sup>

<sup>a</sup> *Dip. di Fisica, Univ. di Milano, and INFN Sez. Milano, Via Celoria 16, Milano, Italy*

<sup>b</sup> *Dept. Theoretical Physics, Univ. Libre de Bruxelles, Bruxelles, Belgium,*

<sup>c</sup> *Dept. Fisica Teorica C-XI, Univ. Autonoma de Madrid, 28049 Madrid, Spain,*

## Abstract

An updated analysis of all available neutrino oscillation evidence in Reactor (Kamland, first 145 days of data) and Solar experiments (SK day and night spectra, global rates from Homestake, SAGE and GALLEX) including the *SNOCC* and *NC* data is presented. In the framework of two active neutrino oscillations we determine the allowed regions in neutrino parameter space, we obtain, from the Kamland spectral shape and global signal, the following antineutrino best solution parameters,  $\Delta m_{kl}^2 = 7.7 \times 10^{-5} eV^2$ ,  $\tan^2 \theta_{kl} = 0.98$ . The overall effect of the measured observed ratio  $R \sim 0.6$  is that the LMA region remains the only one which is still favored.

Combining Kamland and Solar data and assuming CPT invariance, i.e. the same mass matrix for neutrino and antineutrinos, we obtain the following antineutrino best solution parameters (LMAI solution),  $\Delta m^2 = 7.1 \times 10^{-5} eV^2$ ,  $\tan^2 \theta = 0.47$ . A second solution (LMAII) appears for values  $\Delta m^2 = 1.5 \times 10^{-4} eV^2$ ,  $\tan^2 \theta = 0.48$ . We determine additionally individual neutrino mixing parameters and their errors from fits to marginal likelihood distributions, the values are compatible with previous results. In both methods,  $\chi^2$  minimization and marginal likelihood, the combined analysis of solar and Kamland data concludes that maximal mixing is not favored at the  $\sim 3\sigma$  level at least.

PACS: 26.65.+t, 14.60.Pq

\* e-mail: paola.aliانى@cern.ch, vito.antonelli@mi.infn.it, marco.picariello@mi.infn.it, emilio.torrente-lujan@cern.ch

# 1 Introduction

Evidence of antineutrino disappearance in a beam of antineutrinos in the Kamland experiment has been recently presented [1]. The analysis of these results [1, 2] in terms of neutrino oscillations have largely improved our knowledge of neutrino mixing on the LMA region. The results appear to confirm in an independent way that the observed deficit of solar neutrinos is indeed due to neutrino oscillations. The ability to measure the LMA solution, the one preferred by the solar neutrino data at present, “in the lab” puts Kamland in a pioneering situation: after these results there should remain little doubt of the physical reality of neutrino mass and oscillations.

The publication of the SNO results [3, 4] has already made an important breakthrough towards the solution of the long standing solar neutrino [5–7] problem (SNP) possible. These results provide the strongest evidence so far (at least until Kamland improves its statistics) for flavor oscillation in the neutral lepton sector. From the combined analysis of SNO and other solar evidence, one obtains, in the framework of two active neutrino oscillations, the following set of parameters,  $\Delta m_{solar}^2 = 4.5_{-1.4}^{+2.7} \times 10^{-5} eV^2$ ,  $\tan^2 \theta_{solar} = 0.40_{-0.08}^{+0.10}$ . We will see in this work how the evidence from the Kamland measurements improves or modifies these values.

The previous generation of reactor experiments (CHOOZ [8], PaloVerde [9]), performed with a baseline of about 1 km. They have attained a sensitivity of  $\Delta m^2 < 10^{-3} eV^2$  [8, 10] and, not finding any disappearance of the initial flux, they demonstrated that the atmospheric neutrino anomaly [11] is not due to muon-electron neutrino oscillations. The Kamland experiment is the successor of such experiments at a much larger scale in terms of baseline distance and total incident flux. This experiment relies upon a 1 kton liquid scintillator detector located at the old, enlarged, Kamiokande site. It searches for the oscillation of antineutrinos emitted by several nuclear power plants in Japan. The nearby 16 (of a total of 51) nuclear power stations deliver a  $\bar{\nu}_e$  flux of  $1.3 \times 10^6 cm^{-2} s^{-1}$  for neutrino energies  $E_\nu > 1.8$  MeV at the detector position. About 85% of this flux comes from reactors forming a well defined baseline of 139-344 km. Thus, the flight range is limited in spite of using several reactors, because of this fact the sensitivity of Kamland increases by nearly two orders of magnitude compared to previous reactor experiments.

The aim of this work is to study the implications of the recent Kamland results on the determination of the neutrino oscillation parameters, to understand which regions of the parameter space still allowed by the solar neutrino experiments are favored by them. The structure of this work is the following. In section 2 we discuss the main features of Kamland experiment that are relevant for our analysis: The salient aspects of the procedure we are adopting and the results of our analysis are presented and discussed in section 3. Finally, in section 4 we draw our conclusions and discuss possible future scenarios.

## 2 The computation of the expected signals

### 2.1 The Kamland signal

Electron antineutrinos from nuclear reactors with energies above 1.8 MeV are measured in Kamland by detecting the inverse  $\beta$ -decay reaction  $\bar{\nu}_e + p \rightarrow n + e^+$ . The time coincidence, the space correlation and the energy balance between the positron signal and the 2.2 MeV  $\gamma$ -ray produced by the capture of a already-thermalized neutron on a free proton make it possible to identify this reaction unambiguously, even in the presence of a rather large background.

The two principal ingredients in the calculation of the expected signal in Kamland are the reactor flux and the antineutrino cross section on protons. A number of short baseline experiments (See Ref.[12] and references therein) have previously measured the energy spectrum of reactors at distances where oscillatory effects have been shown to be nonexistent. They have shown that the theoretical neutrino flux predictions are reliable within 2% [13]. The effective flux of antineutrinos released by the nuclear plants is a rather well understood function of the thermal power of the reactor and the amount of thermal power emitted during the fission of a given nucleus, which gives the total amount, and the isotopic composition of the reactor fuel which gives the spectral shape. Detailed tables for these magnitudes can be found in Ref. [12]. For a given isotope the energy spectrum can be parametrized by an exponential expression [14] where the coefficients depend on the nature of the fissionable isotope (see Ref.[12] for explicit values). Along the year, between periods of refueling, the total effective flux changes with time as the fuel is expended and the isotope relative composition varies. We take the average of the relative fission yields over the live time as given by the experiment:  $^{235}\text{U} = 57\%$ ,  $^{238}\text{U} = 7.8\%$ ,  $^{239}\text{Pu} = 30\%$ ,  $^{241}\text{Pu} = 5.7\%$ .

In order to obtain the expected number of events at Kamland, we sum the expectations for all the relevant reactor sources weighting each source by its power and distance to the detector (table II in Ref. [12] ), assuming the same spectrum originated from each reactor. We sum over the nearby power reactors, we neglect farther Japanese and Korean reactors and even farther rest-of-the-world reactors which give only a minor additional contribution. The average number of positrons  $N_i$  which are detected per visible energy bin  $\Delta E_i$  is given by the convolution of different quantities:  $\bar{P}$ , the oscillation probability averaged over the distance and power of the different reactors. Expressions for the antineutrino capture cross section are taken from the literature [14, 15]. The matrix element for this cross section can be written in terms of the neutron half-life, we have used the latest published value  $t_{1/2} = 613.9 \pm 0.55$  [16]. The antineutrino flux spectrum, the relative reactor-reactor power normalization which is included in the definition of  $\bar{P}$  and the energy resolution of Kamland are used in addition. We use in our analysis the following expression for the energy

resolution in the prompt positron detection

$$\sigma(E_e) = 0.0062 + 0.065\sqrt{E_e}. \quad (1)$$

This expression is obtained from the raw calibration data presented in Ref.[17]. Note that we prefer to use this expression instead of the much less accurate one given in Ref.[1]. Moreover, we assume a 408 ton fiducial mass and standard nuclear plant power and fuel schedule, we take an averaged, time-independent, fuel composition equal for each detector as given above. Detection efficiency is taken close 100% and independent of the energy [1].

We will not add any background events as they (a total of  $0.95 \pm 0.99$  events which include random coincidences from radioactive decays,  $< 0.01$  evts, and correlated background from cosmic ray muons and neutrons,  $< 0.5$  events,) can be distinguished from the signal with sufficiently high efficiency or are negligible above the 2.6 MeV analysis threshold (table I in Ref. [1]). We also consider negligible the background from geological neutrinos above the 2.6 MeV analysis threshold.

## 2.2 The Solar Signal

We also need the expected signals in the different solar neutrino experiments. These are obtained by convoluting solar neutrino fluxes, sun and earth oscillation probabilities, neutrino cross sections and detector energy response functions. We closely follow the same methods already well explained in previous works [5, 18–20], we will mention here only a few aspects of this computation. We determine the neutrino oscillation probabilities using the standard methods found in literature [21], as explained in detail in [18] and in [5]. We use a thoroughly numerical method to calculate the neutrino evolution equations in the presence of matter for all the parameter space. For the solar neutrino case the calculation is split in three steps, corresponding to the neutrino propagation inside the Sun, in the vacuum (where the propagation is computed analytically) and in the Earth. We average over the neutrino production point inside the Sun and we take the electron number density  $n_e$  in the Sun by the BPB2001 model [31]. The averaging over the annual variation of the orbit is also exactly performed. To take the Earth matter effects into account, we adopt a spherical model of the Earth density and chemical composition [22]. The joining of the neutrino propagation in the three different regions is performed exactly using an evolution operator formalism [21]. The final survival probabilities are obtained from the corresponding (non-pure) density matrices built from the evolution operators in each of these three regions.

In this analysis in addition to night probabilities we will need the partial night probabilities corresponding to the 6 zenith angle bin data presented by SK [23]. They are obtained using appropriate weights which depend on the neutrino impact

parameter and the sagitta distance from neutrino trajectory to the Earth's center, for each detector's geographical location.

### 3 Analysis and Results

In order to study power of the Kamland results for resolving the neutrino oscillation parameter space, we have developed two kind of analysis. In the first case we deal with the Kamland measured global signal. In the second case we include the full Kamland spectrum information. We perform a complete  $\chi^2$  statistical analysis before and after including in addition the up-date solar evidence obtaining the regions in the parameter space which are favored.

#### 3.1 Analysis of the Global rate

The total  $\chi^2$  value is given by the sum of two distinct contributions, that is the one coming from all the solar neutrino data and the contribution of the Kamland experiment:

$$\chi^2 = \chi_{\odot}^2 + \chi_{glob,KL}^2,$$

with

$$\chi_{glob,KL}^2 = \left( \frac{R^{exp} - R^{teo}(\Delta m^2, \theta)}{\sigma_{stat+sys}} \right)^2. \quad (2)$$

The “experimental” signal ratio is  $R^{exp} = 0.611 \pm 0.085 \pm 0.041$  [1], where the first error is statistical and the second one systematic.

The solar neutrino contribution can be written in the following way:

$$\chi_{\odot}^2 = \chi_{glob}^2 + \chi_{SK}^2 + \chi_{SNO}^2. \quad (3)$$

The function  $\chi_{glob}^2$  correspond to the total event rates measured at the Homestake experiment [24] and at the gallium experiments SAGE [25, 26], GNO [27] and GALLEX [28]. We follow closely the definition used in previous works (see Ref.[5] for definitions and Table (1) in Ref.[5] ‘ for an explicit list of results and other references).

The contribution to the  $\chi^2$  from the SuperKamiokande data ( $\chi_{SK}^2$ ) has been obtained by using double-binned data in energy and zenith angle (see table 2 in Ref.[23] and also Ref.[29]): 8 energy bins of variable width and 7 zenith angle bins which include the day bin and 6 night ones. The definition is given by:

$$\chi_{SK}^2 = (\mathbf{R}^{th} - \mathbf{R}^{exp})^t (\sigma_{unc}^2 + \sigma_{cor}^2)^{-1} (\mathbf{R}^{th} - \mathbf{R}^{exp}). \quad (4)$$

The theoretical and experimental  $\mathbf{R}$  quantities are this time matrices of dimension  $8 \times 7$ . The covariance quantity  $\sigma$  is a 4-rank tensor constructed in terms of statistic

errors, energy and zenith angle bin-correlated and uncorrelated uncertainties. The data and errors for individual energy bins for SK spectrum has been obtained from Ref. [23].

The contribution of SNO to the  $\chi^2$  is given by

$$\chi_{\text{spec-SNO}}^2 = \sum_{d,n} (\mathbf{R}^{\text{th}} - \mathbf{R}^{\text{exp}})^t (\sigma_{\text{stat}}^2 + \sigma_{\text{syst}}^2)^{-1} (\mathbf{R}^{\text{th}} - \mathbf{R}^{\text{exp}}), \quad (5)$$

where the day and night  $\mathbf{R}$  vectors of dimension 17 are made up by the values of the total (NC+CC+ES) SNO signal for the different bins of the spectrum. The statistical contribution to the covariance matrix,  $\sigma_{\text{stat}}$ , is obtained directly from the SNO data. The part of the matrix related to the systematical errors has been computed by us studying the influence on the response function of the different sources of correlated and uncorrelated errors reported by SNO collaboration (see table II of Ref. [4]), we assume full correlation or full anticorrelation according to each source.

To test a particular oscillation hypothesis against the parameters of the best fit and obtain allowed regions in parameter space we perform a minimization of the two dimensional function  $\chi^2(\Delta m^2, \tan^2 \theta)$ . A given point in the oscillation parameter space is allowed if the globally subtracted quantity fulfills the condition  $\Delta\chi^2 = \chi^2(\Delta m^2, \theta) - \chi_{\text{min}}^2 < \chi_n^2(CL)$ . Where  $\chi_{n=2}^2(90\%, 95\%, \dots)$  are the quantiles for two degrees of freedom.

In Figs.1 we graphically show the results of this analysis. The favored region by the Kamland global rate alone is presented in fig.1(Left). Fig.1(right) includes the full Kamland and Solar contributions. Kamland global rate alone restricts the value of  $\tan^2 \theta$  to be in the range  $\tan^2 \theta > 4 \times 10^{-1} - 1$  (symmetric with respect the value  $\theta = \pi/4$ ) except for some small region corresponding to  $\tan^2 \theta \sim 1$  and  $\Delta m^2 \sim 2 - 3 \times 10^{-5} \text{ eV}^2$ . The overall effect of the measured observed ratio  $R \sim 0.6\%$  is that the LMA region remains the only one which is still favored. Only if Kamland should had measured a ratio  $\sim 0.1 - 0.3$ , more than three sigma away from the actual measurement, other regions as the LOW solar solution would have some statistical chance to survive. In Table (I.a) we present the best fit parameters or local minima obtained from the minimization of the  $\chi^2$  function. Also shown are the values of  $\chi_{\text{min}}^2$ . According to these results, regardless of the individual Kamland results, a maximal mixing solution is excluded when solar data is included in the analysis.

### 3.2 Analysis including the full Kamland signal

Here we use the binned Kamland signal (See table 2 extracted from Fig.5 in Ref.[1]) combined with the evidence of the up-date solar experiments (CL,GA,SK and SNO). The total  $\chi^2$  value is given now by the sum of two distinct contributions, that is the one coming from all the solar neutrino data and the contribution of the Kamland

experiment which includes both, shape and total signal information:

$$\chi^2 = \chi_{\odot}^2 + \chi_{spec,KL}^2 + \chi_{glob,KL}^2. \quad (6)$$

The contributions of the solar neutrino experiments  $\chi_{\odot}^2$  and global Kamland signal are described in detail in the previous section. The contribution of the Kamland spectrum is now as follows:

$$\chi_{spec,KL}^2 = (\alpha \mathbf{R}^{th} - \mathbf{R}^{exp})^t (\sigma_{unc}^2 + \sigma_{corr}^2)^{-1} (\alpha \mathbf{R}^{th} - \mathbf{R}^{exp}) \quad (7)$$

The total error matrix  $\sigma$  is computed as a sum of assumed systematic deviations,  $\sigma_{sys}/S \sim 6.5\%$ , mainly coming from flux uncertainty (3%), energy calibration and threshold (see table II of Ref. [1] for a total systematic error  $\sim 6.4\%$ ), see also Ref.[12, 17, 30]) and statistical errors. The parameter  $\alpha$  is a free normalization parameter. The effect of systematic sources on individual bin deviations has been computed by us studying the influence on the response function, furtherly we have assumed full correlation among bins.

Note that, as an alternative to the previous formula 7 based on ratios and using and standard  $\chi^2$  expression, we could have directly used the absolute number of events in each bin and applied poissonian statistics formulas. The Kamland collaboration in its published analysis uses a mixed strategy and divides the  $\chi^2$  expression in two parts: it adds a standard  $\chi^2$  contribution corresponding to the global rate to a likelihood contribution which models the statistical significance of the spectrum shape. In this work, where we are interested not only on the Kamland data itself but in combining it with the solar data, we prefer to continue using the familiar expression 7 for various reasons: first, for simplicity, clarity and comparability with previous and future results, second, in the major part of the bins, certainly in the most significant ones, the signal is high enough, and more importantly the errors are small enough, to use the Gaussian approximation. For the large energy bins the signal is strictly zero: its contribution is anyway effectively zero in both approaches. Finally, not less importantly, the possibility of introducing in our approach in a straightforward way the effect of correlated systematic deviations among bins.

The  $\mathbf{R}$  are length 13 vectors containing the binned spectrum (0.425 MeV bins ranging from 2.6 to 8.125 MeV) normalized to the non-oscillation expectations. Theoretical vectors are a function of the oscillation parameters:  $\mathbf{R}^{th} = \mathbf{R}^{th}(\Delta m^2, \theta)$ . The experimental vectors  $\mathbf{R}^{exp}$  contain the Kamland binned signal. We generate acceptance contours (at 90,95 and 99 % CL) in the  $(\Delta m^2, \tan^2 \theta)$  plane in a similar manner as explained in the previous section including now a minimization respect the parameter  $\alpha$  for any of the other oscillation parameters. For the sake of comparison we have also obtained exclusion regions derived from the consideration of the Kamland contribution alone ( $\chi_{KL}^2 = \chi_{spec}^2 + \chi_{gl}^2$ ).

In Figs.(2) we graphically show the results of this analysis. The first case, study of the Kamland data alone ( $\chi^2_{KL}$ ) is represented by the Fig.(2)( left). The allowed regions in parameter space corresponding to each particular point is formed by a number of regions symmetric with respect the line  $\tan \theta = 1$ . The general effect of the inclusion of the solar evidence, showed in Fig.2 (right), in the  $\chi^2$  is the breaking of the symmetry in  $\tan^2 \theta$ , as expected, and the strong contraction of the allowed area to well defined regions. The best fit parameters obtained from the minimization of the  $\chi^2$  function are presented in Table (I.a) where two well separated solutions appear LMAI,LMAII. In both cases the mixing angle is around  $\tan^2 \theta \sim 0.45 - 0.48$ .

Again, the introduction of the solar data strongly diminishes the favored value for the mixing angle. The final value is more near to those values favored by the solar data alone than to the Kamland ones. This effect could be simply due to the present low Kamland statistics or, more worrying, to some statistical artifact derived from the complexity of the analysis and of the heterogeneity of binned data involved.

In this respect, we perform additionally a second kind of analysis in order to obtain concrete values for the individual oscillation parameters and estimates for their uncertainties. We study the marginalized parameter constraints where the  $\chi^2$  quantity is converted into likelihood using the expression  $\mathcal{L} = e^{-(\chi^2 - \chi^2_{min})/2}$ . This normalized marginal likelihood, obtained from the integration of  $\mathcal{L}$  for each of the variables, is plotted in Figs. (3) for each of the oscillation parameters  $\Delta m^2$  and  $\tan^2 \theta$ . For  $\tan^2 \theta$  we observe that the likelihood function is strongly peaked in a region  $\tan^2 \theta \sim 0.4 - 0.6$ . The situation for  $\Delta m^2$  is similar except for the existence of additional, somehow narrower, secondary peaks. Concrete values for the parameters are extracted by fitting one- or two-sided Gaussian distributions to any of the peaks (fits not showed in the plots). In both cases, for angle and the mass difference distributions the goodness of fit of the Gaussian fit to each individual peak is excellent (g.o.f > 99.8%) thus justifying the consistency of the procedure. The values for the parameters obtained in this way appear in Table (I.b). They are fully consistent and very similar to the values obtained from simple  $\chi^2$  minimization. In particular, the maximal mixing solution is again excluded at the  $\sim 3\sigma$  level.

Although both are mutually compatible, the slight difference of the value obtained for the mixing angle is well explained by the shape of the allowed regions in Fig 2 (right): the right elongation of these makes the value of the integral which defines the marginal distribution for  $\tan^2 \theta$  to be shifted. Additional variability can be easily introduced if would have used different prior information or different parameter definition (i.e.  $\sin 2\theta$  instead of  $\tan^2 \theta$ ). This an example of how the details of statistical analysis can significantly modify the values of the physical parameters extracted from data and how important is that different methods are explored, specially in the present context of neutrino physics where heterogeneous data coming from very different sources is jointly used.

## 4 Summary and Conclusions

We have analyzed the present experimental situation of our knowledge of the neutrino mixing parameters in the region of the parameter space that is relevant for solar neutrinos and we have studied in detail how this knowledge has improved with the recent results presented by the reactor experiment Kamland. We show, how, in general, the regions selected by Kamland alone, all symmetric with respect to  $\tan^2 \theta = 1$ , have a large spreadth in the mixing angle. The experiment has, however, a much higher sensitivity to the mass difference parameter.

Kamland global rate alone restricts the value of  $\tan^2 \theta$  to be in the range  $\tan^2 \theta > 4 \times 10^{-1} - 1$  (symmetric with respect the value  $\theta = \pi/4$ ) except for some small region corresponding to  $\tan^2 \theta \sim 1$  and  $\Delta m^2 \sim 2 - 3 \times 10^{-5} \text{ eV}^2$ . The overall effect of the measured observed ratio  $R \sim 0.6\%$  is that the LMA region remains the only one which is still favored. Only if Kamland should had measured a ratio  $\sim 0.1 - 0.3$ , more than three sigma away from the actual measurement, other regions as the LOW solar solution would have some statistical chance to survive.

From the analysis of the Kamland evidence alone, the allowed regions in parameter space corresponding to each particular point is formed by a number regions symmetric with respect the line  $\tan \theta = 1$ . The general effect of the inclusion of the solar evidence in the analysis is the breaking of the symmetry in  $\tan^2 \theta$ , the strong reduction of the area of the allowed regions and, more importantly, the shifting of the value of the best fit mixing angle from being compatible with maximal mixing to more than  $3\sigma$  incompatibility.

In addition to parameter extraction from  $\chi^2$  minimization, we obtain concrete values for the individual oscillation parameters and estimates for their uncertainties from the marginalized likelihood distributions. For  $\tan^2 \theta$  we observe that the likelihood function is concentrated in a region slightly higher than that one obtained from minimization. According to this analysis, maximal mixing is again excluded at the  $3\sigma$  level. The marginal distribution for  $\Delta m^2$  shows clearly the existence of an additional, somehow narrower and much less significant, secondary peaks. Kamland, after only 150 days of data taking, together with the rest of solar experiments is already able to resolve the neutrino mass difference with a high precision of  $\delta \Delta m_{kl+solar}^2 < \pm 0.8$  to be compared with the solar only case where the precision obtained was  $\delta \Delta m_{solar}^2 < \pm 1.5$ . The situation for the other oscillation parameter is worse, from the present data we obtain  $\delta \tan^2 \theta_{kl+solar} < \pm 0.15$ . This precision is comparable, in fact even worse, than the precision attainable from the solar data alone  $\delta \tan^2 \theta_{solar} < \pm 0.10$  [5]. The perspectives of Kamland, after 1-3 years of data taking, together or not with solar evidence, for a much better determination of the mixing angle are not very optimistic (see the results in Ref.[15]). The ability of experiments as BOREXINO to improve the determination of the mixing angle with a smaller error in the near future remains

an open question (see Ref.[32]).

In summary, in the framework of two active neutrino oscillations we obtain, combining Kamland and Solar data and assuming CPT invariance, i.e. the same mass matrix for neutrino and antineutrinos, the following values for neutrino mixing parameters  $\Delta m_{kl}^2 = 7.1 \times 10^{-5} eV^2$ ,  $\tan^2 \theta_{kl} = 0.47$  from  $\chi^2$  minimization (LMAI solution).

## Acknowledgments

We acknowledge the financial support of the Italian MURST and the Spanish CYCIT funding agencies. The numerical calculations have been performed in the computer farm of the Milano University theoretical group.

## References

- [1] K. Eguchi *et al.* [KamLAND Collaboration], Phys. Rev. Lett. **90** (2003) 021802 [arXiv:hep-ex/0212021].
- [2] J. N. Bahcall, M. C. Gonzalez-Garcia and C. Pena-Garay, arXiv:hep-ph/0212147. A. Bandyopadhyay, S. Choubey, R. Gandhi, S. Goswami and D. P. Roy, arXiv:hep-ph/0212146. W. l. Guo and Z. z. Xing, arXiv:hep-ph/0212142. M. Maltoni, T. Schwetz and J. W. Valle, arXiv:hep-ph/0212129. G. L. Fogli, E. Lisi, A. Marrone, D. Montanino, A. Palazzo and A. M. Rotunno, arXiv:hep-ph/0212127. V. Barger and D. Marfatia, arXiv:hep-ph/0212126. G. Barenboim, L. Borissov and J. Lykken, arXiv:hep-ph/0212116.
- [3] Q. R. Ahmad *et al.* [SNO Collaboration], Phys. Rev. Lett. **89**, 011302 (2002) [arXiv:nucl-ex/0204009].
- [4] Q. R. Ahmad *et al.* [SNO Collaboration], Phys. Rev. Lett. **89**, 011301 (2002) [arXiv:nucl-ex/0204008].
- [5] P. Aliani, V. Antonelli, R. Ferrari, M. Picariello and E. Torrente-Lujan, Phys. Rev. D **67** (2003) 013006 [arXiv:hep-ph/0205053].
- [6] A. Strumia, C. Cattadori, N. Ferrari and F. Vissani, arXiv:hep-ph/0205261. A. Bandyopadhyay, S. Choubey, S. Goswami and D. P. Roy, Phys. Lett. B **540**, 14 (2002) [arXiv:hep-ph/0204286]. V. Barger, D. Marfatia, K. Whisnant and B. P. Wood, Phys. Lett. B **537**, 179 (2002) [arXiv:hep-ph/0204253]. J. N. Bahcall, M. C. Gonzalez-Garcia and C. Pena-Garay, arXiv:hep-ph/0204314. S. Pascoli and S. T. Petcov, arXiv:hep-ph/0205022. P. C. de Holanda and A. Y. Smirnov, arXiv:hep-ph/0205241. R. Foot and R. R. Volkas, arXiv:hep-ph/0204265.
- [7] P. Aliani, V. Antonelli, R. Ferrari, M. Picariello and E. Torrente-Lujan, arXiv:hep-ph/0206308. E. Torrente-Lujan, arXiv:hep-ph/9902339. S. Khalil, E. Torrente-Lujan, Egypt. Math. Soc.
- [8] M. Apollonio *et al.*, CHOOZ Coll., Phys. Lett. **B 466**, 415 (1999)
- [9] Y. F. Wang [Palo Verde Collaboration], Int. J. Mod. Phys. A **16S1B**, 739 (2001); F. Boehm *et al.*, Phys. Rev. D **64**, 112001 (2001) [arXiv:hep-ex/0107009].
- [10] M. Apollonio *et al.* (CHOOZ coll.), hep-ex/9907037, Phys. Lett. **B 466** (1999) 415. M. Apollonio *et al.*, Phys. Lett. **B 420** (1998) 397. F. Boehm *et al.*, Phys. Rev. **D62** (2000) 072002 [hep-ex/0003022].
- [11] K. S. Hirata *et al.* [Kamiokande-II Collaboration], Phys. Lett. B **280**, 146 (1992). T. Toshito [SuperKamiokande Collaboration], arXiv:hep-ex/0105023; Y. Fukuda *et al.* [Super-Kamiokande Collaboration], Phys. Rev. Lett. **81**, 1562 (1998)

- [arXiv:hep-ex/9807003]; R. Becker-Szendy *et al.*, Nucl. Phys. Proc. Suppl. **38**, 331 (1995); M. Sanchez [Soudan-2 Collaboration], Int. J. Mod. Phys. A **16S1B**, 727 (2001); M. Ambrosio *et al.* [MACRO Collaboration], arXiv:hep-ex/0206027.
- [12] H. Murayama and A. Pierce, Phys. Rev. D **65** (2002) 013012 [arXiv:hep-ph/0012075].
- [13] A. Piepke [Kamland collaboration], Nucl. Phys. Proc. Suppl. **91**, 99 (2001)
- [14] P. Vogel and J. F. Beacom, Phys. Rev. D **60**, 053003 (1999) [arXiv:hep-ph/9903554].
- [15] P. Aliani, V. Antonelli, M. Picariello and E. Torrente-Lujan, New J. Phys. **5** (2003) 2 [arXiv:hep-ph/0207348]. P. Aliani, V. Antonelli, R. Ferrari, M. Picariello and E. Torrente-Lujan, AIP Conf. Proc. **655** (2003) 103 [arXiv:hep-ph/0211062]. P. Aliani, V. Antonelli, M. Picariello and E. Torrente-Lujan, JHEP **0302** (2003) 025 [arXiv:hep-ph/0208089]. P. Aliani, V. Antonelli, R. Ferrari, M. Picariello and E. Torrente-Lujan, arXiv:hep-ph/0206308. E. Torrente-Lujan, JHEP **0304** (2003) 054 [arXiv:hep-ph/0302082].
- [16] “Review of Particle Properties”, K. Hagiwara *et al.* (Particle Data Group), Phys. Rev. D **66** (2002) 010001
- [17] G.Horton-Smith, *Neutrinos and Implications for Physics Beyond the Standard Model*, Stony Brook, Oct. 11-13, 2002. <http://insti.physics.sunysb.edu/itp/conf/neutrino.html>  
A.Suzuki. *Texas in Tuscany, XXI Symposium on Relativistic Astrophysics* Florence, Italy, December 9-13, 2002. <http://www.arcetri.astro.it/texaflor/>.
- [18] P. Aliani, V. Antonelli, M. Picariello and E. Torrente-Lujan, Nucl. Phys. **B634** (2002) 393-409. arXiv:hep-ph/0111418.
- [19] P. Aliani, V. Antonelli, M. Picariello and E. Torrente-Lujan, Nucl. Phys. Proc. Suppl. **110**, 361 (2002) [arXiv:hep-ph/0112101].
- [20] P. Aliani, V. Antonelli, R. Ferrari, M. Picariello and E. Torrente-Lujan, arXiv:hep-ph/0205061.
- [21] E. Torrente-Lujan, Phys. Rev. D **59** (1999) 093006 [arXiv:hep-ph/9807371]. E. Torrente-Lujan, Phys. Rev. D **59** (1999) 073001; E. Torrente-Lujan, Phys. Lett. B **441**, 305 (1998); V. B. Semikoz and E. Torrente-Lujan, Nucl. Phys. B **556**, 353 (1999); E. Torrente-Lujan, arXiv:hep-ph/0210037. S. Khalil and E. Torrente-Lujan, J. Egyptian Math. Soc. **9**, 91 (2001) [arXiv:hep-ph/0012203]. E. Torrente Lujan, Phys. Rev. D **53**, 4030 (1996). B. C. Chauhan, J. Pulido and E. Torrente-Lujan, arXiv:hep-ph/0304297.
- [22] I. Mocioiu and R. Shrock, Phys. Rev. D **62** (2000) 053017 [arXiv:hep-ph/0002149].

- [23] M. B. Smy, arXiv:hep-ex/0202020.
- [24] R. Davis, Prog. Part. Nucl. Phys. 32 (1994) 13; B.T. Cleveland et al., (HOMESTAKE Coll.) Nucl. Phys. (Proc. Suppl.) **B 38** (1995) 47; B.T. Cleveland et al., (HOMESTAKE Coll.) Astrophys. J. 496 (1998) 505-526; K. Lande (For the Homestake Coll.) Nucl. Phys. B(Proc. Suppl.) **77**(1999)13-19.
- [25] A.I. Abazov et al. (SAGE Coll.), Phys. Rev. Lett. **67** (1991) 3332; D.N. Abdurashitov et al. (SAGE Coll.), Phys. Rev. Lett. **77** (1996) 4708; J.N. Abdurashitov et al., (SAGE Coll.), Phys. Rev. **C60** (1999) 055801; astro-ph/9907131; J.N. Abdurashitov et al., (SAGE Coll.), Phys. Rev. Lett. **83** (1999) 4686; astro-ph/9907113. J. N. Abdurashitov *et al.* [SAGE Collaboration], of solar activity,” arXiv:astro-ph/0204245.
- [26] J.N. Abdurashitov et al. (SAGE Coll.) Phys. Rev. Lett. 83(23) (1999)4686.
- [27] M. Altmann et al. (GNO Coll.) Phys. Lett. B490 (2000) 16-26.
- [28] P. Anselmann et al., GALLEX Coll., Phys. Lett. **B 285** (1992) 376; W. Hampel et al., GALLEX Coll., Phys. Lett. **B 388** (1996) 384; T.A. Kirsten, Prog. Part. Nucl. Phys. 40 (1998) 85-99; W. Hampel et al., (GALLEX Coll.) Phys. Lett. **B 447** (1999) 127; M. Cribier, Nucl. Phys. (Proc. Suppl.) **B 70** (1999) 284; W. Hampel et al., (GALLEX Coll.) Phys. Lett. **B 436** (1998) 158; W. Hampel et al., (GALLEX Coll.) Phys. Lett. **B 447** (1999) 127.
- [29] S. Fukuda *et al.* [Super-Kamiokande Collaboration], Phys. Lett. B **539**, 179 (2002) [arXiv:hep-ex/0205075].
- [30] J. Shirai, “Start of Kamland”, talk given at *Neutrino 2002*, XXth International Conference on Neutrino Physics and Astrophysics, May 2002, Munich. Transparencies can be obtained from <http://neutrino2002.ph.tum.de>. See also: P. Alivisatos *et al.*, STANFORD-HEP-98-03.
- [31] J. N. Bahcall, M. H. Pinsonneault and S. Basu, Astrophys. J. **555**, 990 (2001) [arXiv:astro-ph/0010346].
- [32] P. Aliani, V. Antonelli, M. Picariello and E. Torrente-Lujan, To appear.

	$\Delta m^2(eV^2)$	$\tan^2 \theta$	$\chi_{min}^2$
Table I.a (Minimization $\chi^2$ ):			
KL (Sp)	$7.7 \times 10^{-5}$	0.98	1.93
KL (Gl)+Solar	$5.8 \times 10^{-5}$	0.47	45.8
KL (Sp+Gl)+Solar, LMAI	$7.1 \times 10^{-5}$	0.47	49.1
KL (Sp+Gl)+Solar, LMAII	$1.5 \times 10^{-4}$	0.48	49.8
Table I.b ( From Fit, Fig.3, $\pm 1\sigma$ ):			
KL (SP+Gl)+Solar, LMAI	$8.0^{+0.9}_{-0.8} \times 10^{-5}$		
KL (SP+Gl)+Solar, LMAII	$1.7^{+0.2}_{-0.2} \times 10^{-4}$		
KL (SP+Gl)+Solar		$0.55^{+0.16}_{-0.12}$	

Table 1: Mixing parameters: From  $\chi^2$  minimization (Tables I.a) and from fit to the peak of marginal likelihood distributions (Table I.b).

Bin (MeV)	$R = S_{exp}/S_{MC}$	$\pm 1\sigma_{stat}$
2.600-3.025	0.435	$\pm 0.160$
3.025-3.450	0.689	$\pm 0.215$
3.450-3.875	0.666	$\pm 0.225$
3.875-4.300	0.719	$\pm 0.250$
4.300-4.725	0.885	$\pm 0.310$
4.725-5.150	0.550	$\pm 0.305$
5.150-5.575	1.000	$\pm 0.460$
5.575-6.000	0.598	$\pm 0.500$
6.000-6.425	0.000	$\pm 0.365$
6.425-6.850	0.000	$\pm 0.630$
6.850-7.275	0.000	$\pm 2.500$
7.275-7.700	0.000	$\pm 2.500$
7.700-8.125	0.000	$\pm 2.500$

Table 2: Summary of Kamland signal ratios as used in the present work. The table has been obtained from the information contained in Fig.5 in Ref.[1].

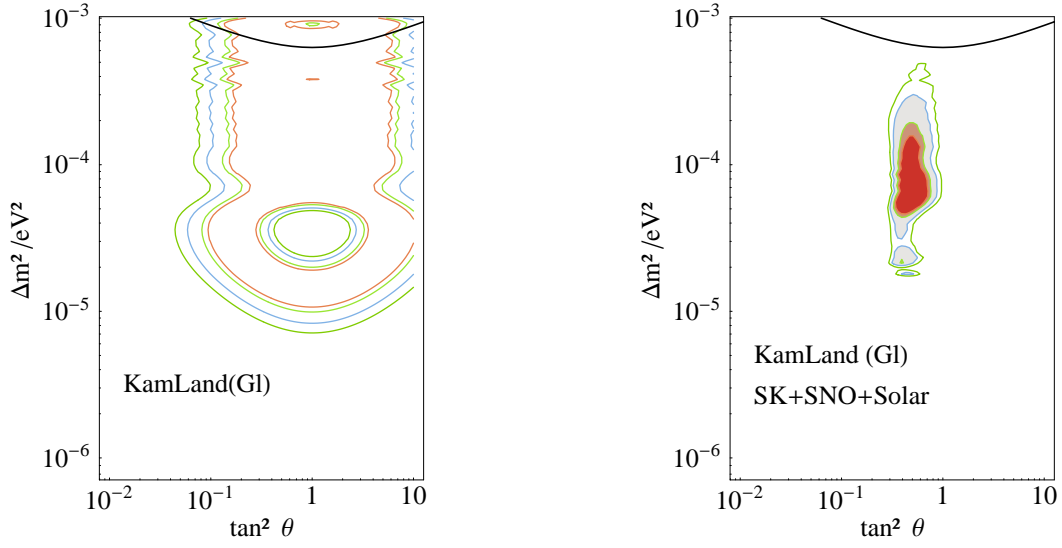


Figure 1: Exclusion plots including Kamland global rates. The colored areas are allowed at 90, 95, 99 and 99.7% CL relative to the absolute minimum. The region above the upper thick line is excluded by the previous CHOOZ experiment [10].

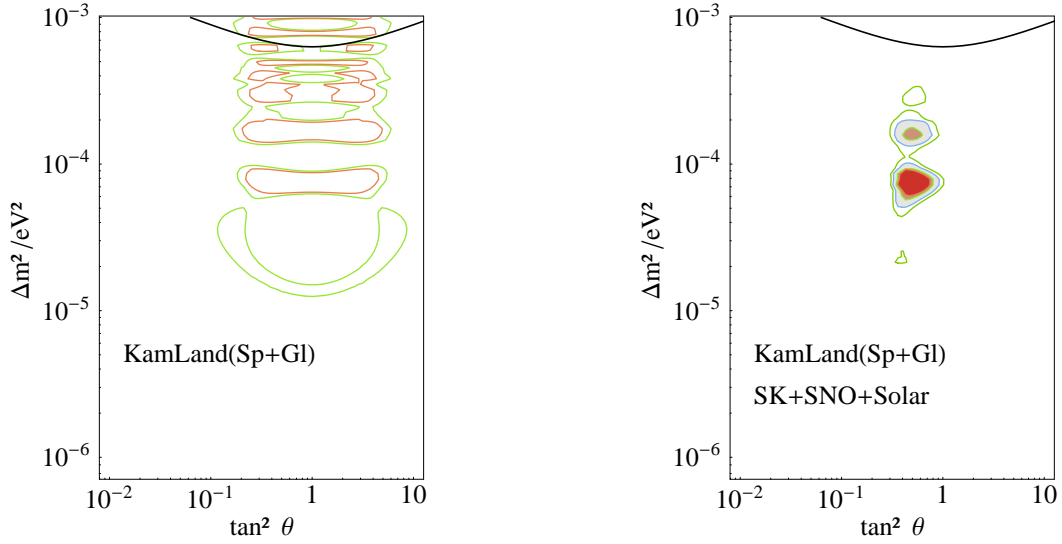


Figure 2: Allowed areas in the two neutrino parameter space after 150 days of data taking in Kamland. The colored lines separate allowed regions at 90, 95, 99 and 99.7% CL relative to the absolute minimum. (Left) Results with the Kamland signal alone (shape and total signal information, only 90,95% Cl lines are shown for clarity). (Right) Kamland spectrum plus solar (CL,GA,SK,SNO) evidence.

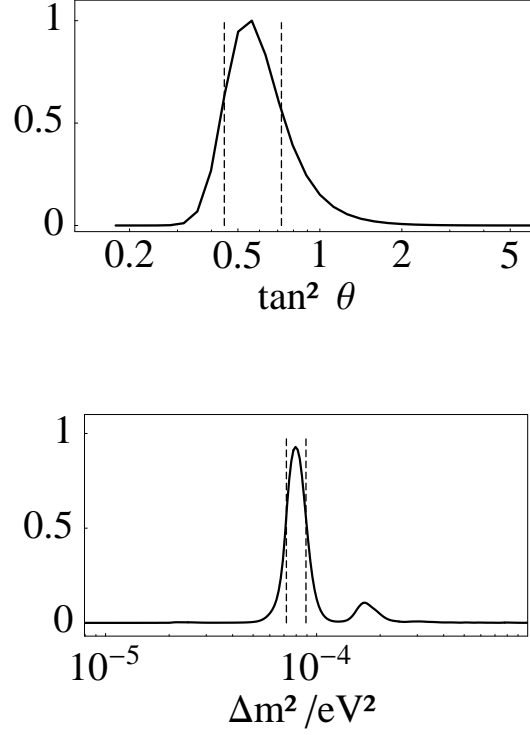


Figure 3: Marginalized likelihood distributions for each of the oscillation parameters  $\Delta m^2$  (right),  $\tan^2 \theta$  (left) corresponding to the Kamland Spectrum plus solar evidence (Fig.2(Right)). The curves are in arbitrary units with normalization to the maximum height. Values for the peak position are obtained by fitting two-sided Gaussian distributions (not showed in the plot). Dashed lines delimit  $\pm 1\sigma$  error regions around the maximum. See Table I.a for values of the position and widths of the peaks.